ChemElectroChem

Research Article
doi.org/10.1002/celc.202201152

Chemistry Europe
European Chemical Societies Publishing

www.chemelectrochem.org

Flexible and Binder-Free Iron Phosphide Electrodes Using a Three-Dimensional Support for High Hydrogen Productivity

María Isabel Díez-García,*[a, b] Andrés Alberto García Blanco,[a, c] Sebastian Murcia-López,[a] Marc Botifoll,[d] Jordi Arbiol,[d, e] Mohammad Qamar,[f] and Joan Ramon Morante[a]

In this work, an inexpensive and reliable microstructured electrode for the hydrogen evolution reaction (HER) is developed. This cathode is made of Earth-abundant elements consisting of iron phosphide as an electrocatalyst and carbon felt (CF) as a flexible conductive scaffold. Its porous character and binder-free FeP coverage over the carbon fibers generate a high number of accessible active sites for the reaction, achieving a high value of the electrochemically active surface area. The electrode reaches 100 $mA \cdot cm^{-2}$ by applying only −53 mV vs RHE at 50 °C in 0.5 M H_2SO_4, demonstrating excellent electrocatalytic activity for the HER and outstanding stability in acidic electrolyte. Furthermore, the feasibility of these electrodes for industrial application is evaluated using a PEM electrolyzer. The developed prototype with a cathodic area of 1.8 cm^2 shows a very promising performance, reaching 14.9 mmol $H_2 \cdot h^{-1} \cdot cm^{-2}$ (corresponding to 800 $mA \cdot cm^{-2}$) at a voltage of only 2.1 V.

Introduction

The deployment of carbon-free energy technologies that are competing with the price of fossil fuels, is expected to be a key factor in sustaining the future energy requirements of the world population. In this regard, H_2 is a promising energy vector with a high energy density that can be produced electrochemically from pure water with zero carbon emissions. The required input power for the water splitting reaction in an electrolyzer can be obtained from renewable sources, such as wind, solar, geothermal or hydraulic energy. Additionally, the development of efficient devices needs cost-effective, high productivity and stable electrocatalysts as well as minimum energy input to drive the electrochemical reactions (i.e., low overpotentials). Under this scenario, in addition to the electrocatalytic activity of the material, other key parameters must also be considered such as the electrode structure and the cell configuration. They are critical for fast electron transfer in the electrocatalyst/electrolyte interface, and for avoiding mass transport limitations by assuring appropriate product (gas) release through the nano/microporous structure. In this work, we have paid attention to these design issues through the fabrication of an inexpensive 3D electrode made of Earth-abundant elements, such as FeP and a carbonaceous supporting scaffold (carbon felt). Likewise, concerning the cell configuration, a proton exchange membrane electrolyzer (PEM electrolyzer),[1–4] which presents some advantages over the traditional electrolysis technologies, has been selected.

Commonly, Pt is one of the materials leading the benchmark electrocatalytic activity for hydrogen evolution reaction (HER). In fact, commercial PEM electrolyzers are based on Pt and Ir, but they are expensive and scarce elements. This motivates the research of other cost-effective materials made of Earth-abundant elements with competitive catalytic activities compared to precious metal-based catalysts. Some transition metal compounds such as hydroxides, oxides, carbides, sulfides, phosphides and nitrides have demonstrated promising electrocatalytic activity for the HER.[5] Among them, transition metal phosphides have attracted attention because most of them exhibit favorable properties such as electrical and thermal conductivity,[6] with similar values to those expected for compounds with metallic character, which make them advantageous against other electrocatalytic active materials.

Therefore, metal phosphides based on Co, Mo, Ni and Fe have been widely studied for the HER.[7–10] For a high performance not only the nature of the electrocatalyst is important but also its interaction with the conductive scaffold. In the last years, new synthesis procedures that are advantageous against previous general approaches, such as the trioctylphosphine (TOP) route, have been developed.[7,11,12] Among these materials,

[a] Dr. M. I. Díez-García, Dr. A. A. García Blanco, Dr. S. Murcia-López, Prof. J. R. Morante
Catalonia Institute for Energy Research (IREC)
Jardins de les Dones de Negre 1, 08930 Sant Adrià del Besòs, Barcelona (Spain)
E-mail: midiez@irec.cat
[b] Dr. M. I. Díez-García
Current address:
École Polytechnique Fédérale de Lausanne
Station 6, 1015 Lausanne (Switzerland)
E-mail: maria.diezgarcia@epfl.ch
[c] Dr. A. A. García Blanco
Instituto de Física Aplicada (INFAP-CONICET)
Universidad Nacional de San Luis
Av. Ejército de los Andes 950, San Luis 5700 (Argentina)
[d] M. Botifoll, Prof. J. Arbiol
Catalan Institute of Nanoscience and Nanotechnology (ICN2)
CSIC and BIST, Campus UAB Bellaterra, 08193 Barcelona, Catalonia (Spain)
[e] Prof. J. Arbiol
ICREA
Pg. Lluís Companys 23, 08010 Barcelona, Catalonia (Spain)
[f] Dr. M. Qamar
Interdisciplinary Research Center for Hydrogen and Energy Storage
King Fahd University of Petroleum and Minerals
Dhahran 31261 (Saudi Arabia)

Supporting information for this article is available on the WWW under https://doi.org/10.1002/celc.202201152

iron phosphide (FeP) is a promising candidate as Fe is one of the most abundant elements in the Earth's crust, and its electrocatalytic activity for the HER has been reported in different electrolytes.[5,13,14] More recently, DFT studies have revealed appropriate Gibbs free energies of hydrogen adsorption in some FeP facets,[15,16] which contributes to the excellent performance of this material.[8] Kwong et al.[17] pointed out that cationic vacancy defects (Fe vacancies) in FeP increase the HER activity by modulating hydrogen absorption. The stability of FeP has been reported extensively at low current densities in acidic media,[5] while in alkaline media some reports pointed out instability evidenced by some drop of the current with time at a current density of 10 $mA \cdot cm^{-2}$.[18,19] Furthermore, the synthesis of FeP via the decomposition of sodium hypophosphite is simple, scalable and provides more flexibility in the use of different metal precursors. Additionally, the morphology is preserved after the phosphidization step,[7,14] allowing more control over the ultimate structure and the electrocatalyst/substrate configuration. This facilitates the direct growth of FeP on the scaffolds without extra additives that may hinder electron transport,[20,21] or block the active sites[14] thereby decreasing the catalytic activity.

On the other hand, the use of carbonaceous scaffolds is advisable in practical electrolyzers as they are generally highly conductive and relatively cost-effective. Previously, the electrocatalytic activity of FeP deposited on carbon nanostructures[22] and other carbon scaffolds such as carbon cloth[14,22–25] have been studied. Carbon felt (CF) is composed of carbon fibers with a micrometric diameter that may be favorable for the mass transport of the produced gases and homogenous composition inside the pores, especially when the hydrogen production rates are high. CF is reported as robust support for large-scale production because of its adequate electrical conductivity, macroporous structure, chemical stability, and high surface area.[26] In fact, because of these favorable properties, it is extensively employed in redox flow battery devices.[27] Importantly, carbon felt can be pressed against the membrane for zero-gap configuration in a PEM flow cell, which is facilitated by the soft and compressible nature of this substrate.

In this work, we report on the fabrication of FeP-based cathodes using CF as conductive support. We followed a route based on the direct growth of tiny FeP nanoparticles on the 3D structure of the CF that avoids the use of binders, facilitating the charge transfer and favoring the exposure of a high number of active sites.[12] Firstly, Fe_2O_3 is deposited on the carbon microstructures and afterward converted to FeP by a reaction at relatively low temperatures in presence of NaH_2PO_2. The adequate electrocatalyst/scaffold configuration led to a high electroactive area and good electron transport that derived, considering also the electrocatalyst characteristics, in optimized overpotentials for the HER. Then, these cathodes have been tested at a high current density at 50 °C, which is close to the operative temperatures used in commercial electrolyzers. The feasibility of the synthesis route and the flexibility of the CF substrate facilitate the integration of the FeP-based cathode in a PEM electrolyzer under flow cell conditions.

Results and Discussion

Physicochemical characterization of the FeP/CF electrodes before HER

The electrodes were characterized by XRD before and after the heat treatment at 350 °C in presence of NaH_2PO_2. Figure 1a shows that, after annealing at 400 °C in air, the diffraction peaks match with those of the hematite phase (JCPDS 01-072-0469). The crystallite size calculated by the Scherrer equation in the peak of the plane (1 1 0) is 22 nm. The Fe_2O_3/CF electrodes were converted to FeP by the reaction with PH_3, generated in situ by thermal decomposition of the sodium hypophosphite

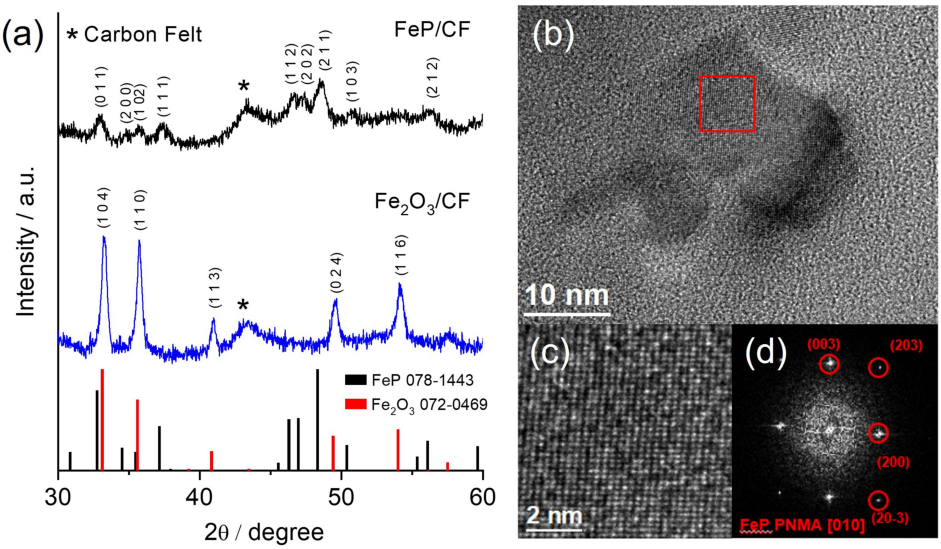

Figure 1. (a) XRD patterns of the Fe_2O_3/CF (after the annealing at 400 °C in air) and the as-prepared FeP/CF electrode after phosphidization at 350 °C. The peak positions according to the JCPDS cards 078-1443 and 072-0469 for FeP and Fe_2O_3, respectively, are included at the bottom of the graph. (b) HRTEM image of an FeP crystal from the FeP/CF electrode after the acid etching, the magnification of the red squared area in (c) and its FFT spectrum in (d).

at 350 °C: 2 $NaH_2PO_2 \cdot H_2O \rightarrow PH_3 + Na_2HPO_4 + H_2O$.[28] After the phosphidization step, the XRD pattern confirms the transformation of Fe_2O_3 into the orthorhombic phase of FeP (JCPDS 01-078-1443). The crystallite size decreased after phosphidization to 11 nm, calculated from the plane (2 1 1) of FeP. It should be mentioned that after the acid etching treatment, which is performed before the electrochemical tests to remove some impurities derived from the synthesis, the XRD pattern also shows the peaks ascribed to FeP, as expected. The plane (100) of graphitic carbon is also present in the XRD patterns, in agreement with the spectra of the bare carbon felt (Figure S1).[26] The morphology of the FeP/CF electrode was analyzed by HRSEM. Figure S2a–c show the carbon fibers covered by the FeP nanoparticles. In general, the coalescence of these nanoparticles forming a porous layer is observed in some regions (see Figures S2b–c). Such morphological features give rise to a high surface area and consequently high surface reaction sites while the macropores are still preserved. This is beneficial to avoid diffusion limitations, especially for the release of the hydrogen bubbles produced and at the same time, the mass transport through the electrolyte is guaranteed.

To get more insights into the crystalline structure of FeP nanocrystals, the electrodes after the acid etching were analyzed by high-resolution transmission electron microscopy (HRTEM). Figure 1b–c show a nanoparticle of about 20 nm with well-defined lattice fringes oriented along the [010] direction. Figure 1d displays the Indexed Power spectrum (Fast Fourier transform (FFT)) obtained in the red squared region of Figure 1b (and the magnification of this area in Figure 1c) that agrees with the orthorhombic phase (PNMA space group 62) of FeP. This crystalline phase is in agreement with the XRD results in Figure 1a. The [010] facet has been identified as active for the HER according to DFT calculations and experimental results.[29,30] Other facets were also identified in the electrode by applying FFT (Figure S3) in agreement with the nanoparticulated morphology of the electrocatalyst. Electron energy-loss spectroscopy (EELS) analysis in Figure 2 shows a homogeneous distribution of Fe and P throughout the particles. Oxygen was also detected but with very low intensity indicating that some undesired oxygenated species can be present as impurities. Thus, it can be concluded that the deposited electrocatalyst is mostly composed of nanoparticles of FeP.

Electrochemical characterization of the FeP/CF electrodes in three-electrode configuration

The electrocatalytic activity of the FeP/CF electrodes for the HER was evaluated in 0.5 M H_2SO_4 and 1 M KOH. Figure 3a-b show the polarization curves after IR correction. The respective overpotentials for the FeP/CF electrode in the acidic electrolyte at room temperature are calculated to be 41, 55 and 97 mV to produce 10, 20 and 100 $mA \cdot cm^{-2}$. As a reference test, the electrochemical response of the bare CF substrate using the same tantalum-based electrical contact was also measured to evaluate the activity of the HER in the selected potential range. The CF was exposed to the same heat treatments as those of the FeP/CF electrodes, but without being immersed in the iron precursor solution. Figure S4 shows that the CF produces much lower currents below 0 V vs RHE than the FeP/CF electrode, ruling out any significant contribution of the supporting material and the metallic contact to the HER activity. In the alkaline electrolyte, the overpotentials are higher than those recorded under acidic conditions, which is a typical behavior in the HER electrocatalysis. Water dissociation takes place before hydrogen adsorption in alkaline media, which generally makes HER reaction more sluggish[31,32] Figure 3b shows the linear sweep voltammetry for the FeP/CF in 1 M KOH electrolyte and the overpotentials are 63, 82 and 123 mV for producing 10, 20 and 100 $mA \cdot cm^{-2}$, respectively. The electrochemical activity for the HER obtained in this study is among the best reported in the literature in both electrolytes, including electrodes prepared

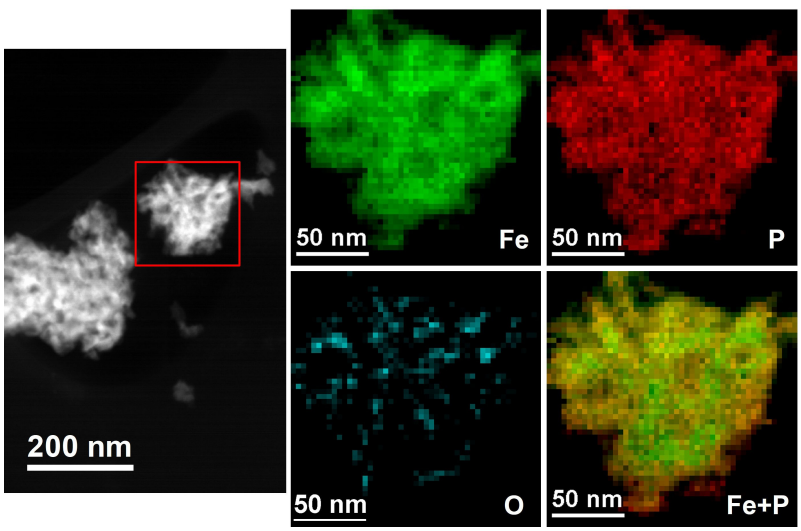

Figure 2. EELS maps of Fe, P, O and Fe + P in the red squared area marked in the STEM-ADF image (on the left side) of an FeP nanoparticle from an acid-etched FeP/CF electrode.

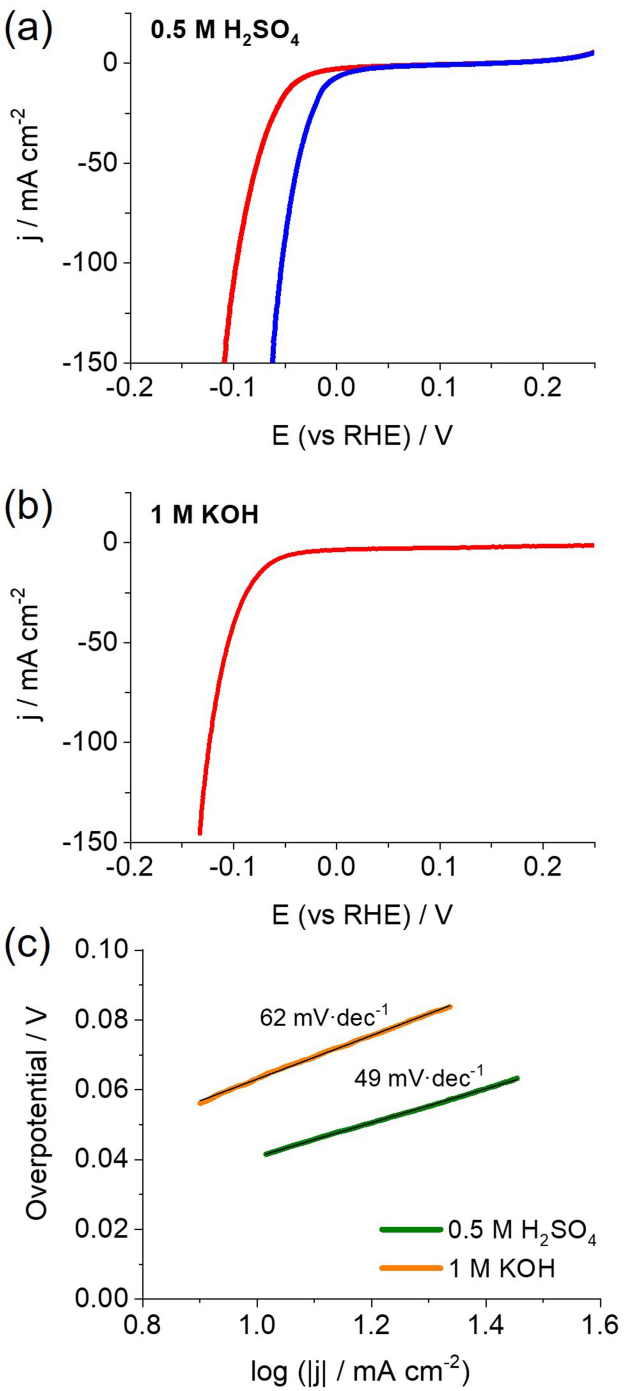

Figure 3. Linear sweep voltammograms (negative-going scans) in (a) 0.5 M H_2SO_4 and (b) 1 M KOH at 25 °C (red lines) and 50 °C (blue line), and (c) Tafel plots at 25 °C in both electrolytes for FeP/CF electrodes.

by the direct deposition of the electrocatalysts on porous substrates (see Tables S1 and S2).

The determination of the Tafel slopes helps to obtain insights into the reaction mechanisms. Thus, Tafel plots in Figure 3c are obtained from the cyclic voltammetries in Figure 3a–b. At room temperature, Tafel slopes in acidic and alkaline electrolytes are estimated to be 49 and 62 $mV \cdot dec^{-1}$, respectively. Such values suggest a Volmer-Heyrovsky mechanism in both cases, being the limiting reaction step the Heyrovsky step. This reaction mechanism is the most reported for the HER catalyzed by FeP in both electrolytes,[25,33–35] except few reports that point out a Volmer-Tafel mechanism.[23,24] The FeP/CF electrodes show high exchange current densities (j_0) of 1.44 and 0.98 $mA \cdot cm^{-2}$ in the acidic and alkaline electrolytes, respectively. This parameter was estimated from the intercept with the x-axis in the Tafel plots (Figure 3c) obtained from the extrapolation of the linear region. For direct deposition of FeP, the j_0 recorded in this study is one of the highest values reported in the literature (see Tables S1 and S2).

When the temperature is increased to 50 °C (Figure 3a) in the acidic electrolyte, the potentials after IR correction are reduced by 33, 35 and 44 mV for 10, 20 and 100 $mA \cdot cm^{-2}$ with respect to those obtained at 25 °C. This enhancement in the HER activity with the temperature can be correlated with a shift of the intercept with the x-axis toward higher values in the Tafel plot, which is linked to a higher j_0 (Figure S5a). A higher exchange current density is related to improved kinetics of the HER.[36] On the contrary, in alkaline media, there is only a slight change of the overpotentials at 50 °C (Figure S5b) in comparison with those at room temperature (Figure 3b). This behavior may be related to some changes in the electrode upon increasing the temperature in this electrolyte.

The ECSA (electrochemically active surface area) is determined to get insights into the electrode characteristics leading to high electrocatalytic activity. It can be estimated through the value of the double-layer capacitance, C_{dl}, (see ECSA determination section in the SI for details),[37] which can be determined from the values of the capacitive current densities as a function of the scan rate.[32] Herein, the potential limits for the cycles were set between −0.2 and 0.05 V vs Ag/AgCl in 0.5 M H_2SO_4 (Figure S6). From Figure 4a, C_{dl} was estimated to be 190 $mF \cdot cm^{-2}$ for an FeP/CF electrode. Considering a reference double-layer capacitance value of 40 $\mu F \cdot cm^{-2}$ for a planar surface,[29,32] the ECSA for the FeP/CF electrode can be estimated to be about 4700 cm^2 per cm^2 of geometric area. Remarkably, the C_{dl} value is 1–2 orders of magnitude higher than others reported for metal phosphides.[38] The impressive ECSA value is a result of the high porosity and thickness of the electrode and the nanoparticulated morphology of the deposited electrocatalyst. These results point out the suitability of the employed synthetic method for achieving a homogenous deposition of the FeP throughout all the carbon fibers while having wide pores for assuring good wettability of the whole electrode and good hydrogen release. The linear sweep voltammetry displaying the current density normalized by ECSA is presented in Figure S7.

Another relevant kinetic parameter for evaluating the electrocatalytic activity of the FeP/CF electrode is the turnover frequency (TOF), which represents the number of product molecules generated per active site (N_{act}) in unit time.[32] The determination of an accurate value of N_{act} is challenging and depends on the method employed.[39] One extended method is based on the analysis of the pair of redox peaks appearing in the cyclic voltammetry between −0.2 and 0.6 V vs RHE in 1 M PBS.[32] It should be noted that this method considers the metal sites as the active sites for the reaction in transition metal-based

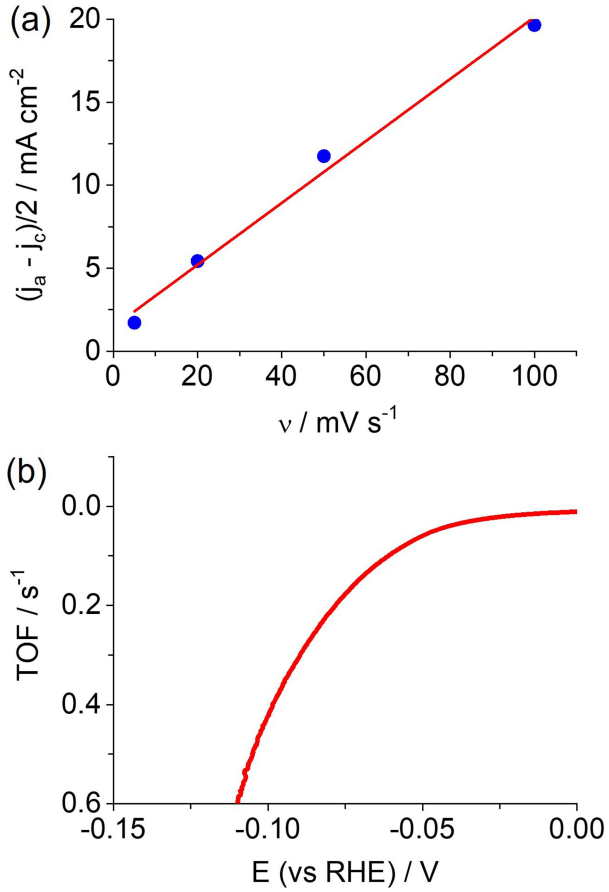

Figure 4. (a) Capacitive currents, $(j_a-j_c)/2$, as a function of the scan rate and (b) TOF values as a function of the potential in 0.5 M H_2SO_4 electrolyte for an FeP/CF electrode.

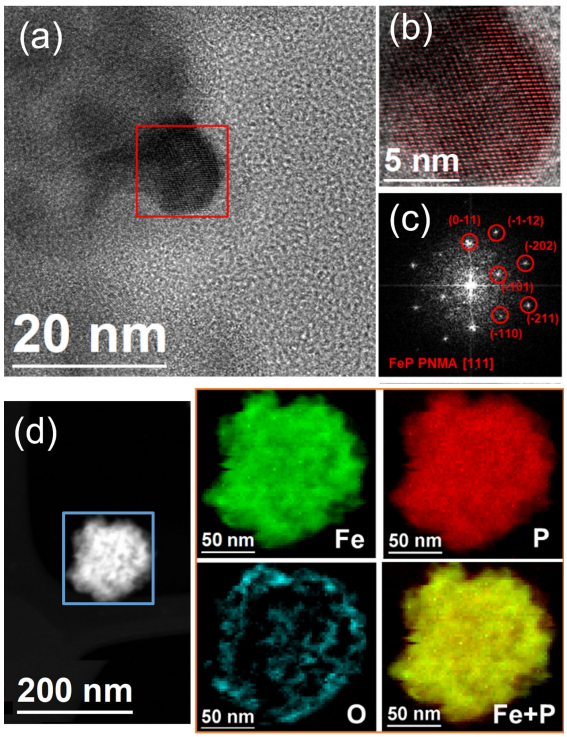

Figure 5. (a) HRTEM image of an FeP crystal from the FeP/CF electrode after HER at 100 mA·cm^{-2} in 0.5 M H_2SO_4 together with the magnification of the area squared in red in (b) and the FFT spectrum in (c). (d) The EELS maps of Fe, P, O and Fe + P in the blue squared area marked in the STEM-ADF image on the left side for an FeP nanoparticle.

electrocatalysts.[39] Assuming a one-electron transfer process related to the redox peaks, the number of active sites is estimated to be $8.1\cdot10^{17}$ per geometric cm^2 (Figure S8 and Eq. S2). Figure 4b displays the TOF values for the HER calculated by Eq. S1 for an FeP/CF electrode. TOF is approximately 0.42 molecules H_2 s^{-1} at an overpotential of 100 mV, which is a comparable value to those obtained for high-performing metal phosphides for the HER.[7,38] These results support the high catalytic activity of the fabricated FeP electrocatalyst anchored in the 3D scaffold.

The FeP/CF electrodes were also characterized after 30 min at a cathodic current of around 100 mA·cm^{-2} (after HER). Figure 5a shows an HRTEM image of an FeP nanocrystal, and a magnification of the red squared area in Figure 5b. The FFT pattern identified in Figure 5c confirms that the particle is composed of FeP PNMA crystal phase, according to the previous analysis before HER (Figure 1a and d). The EELS analysis in Figure 5d shows a homogenous distribution of the Fe and P elements through the particles. From Figure S9, the concentration of Fe and P results in 55(±2)% of Fe and 45(±2)% of P (Fe:P = 1.22:1), which is near the stoichiometric ratio with a slight excess of Fe.

To gain knowledge about the surface composition of the FeP/CF electrodes during HER, they were analyzed by XPS after 30 min at a cathodic current of around 100 mA·cm^{-2}. During this period, any significant current decay was observed. Figure S10 shows the XPS surveys for both electrolytes in which the corresponding signals of Fe 2p, P 2p, C 1s and O 1s can be identified. Importantly, after HER in both electrolytes, the P 2p region in Figure 6a-b displays two peaks at 129.6 and 130.4 eV that correspond to the $2p_{3/2}$ and $2p_{1/2}$ signals of phosphorous bonded to iron as iron phosphide.[14,18] Additionally, a peak near 133.5 eV in the P 2p region appears in both cases. This peak is correlated with PO_4^{3-} that is typically detected at the surface of transition metal phosphides due to partial oxidation upon air exposure.[13,40–42] The Fe 2p spectra in Figure S11 display two peaks at 707.5 eV and 720.3 eV that correspond to the Fe $2p_{3/2}$ and $2p_{1/2}$ doublet ascribed to iron bounded to phosphorous in FeP,[13,18] while the other peaks are associated to iron phosphates (according with the presence of the intense peak of PO_4^{3-} in the P 2p region) or other oxygenated species. In fact, the bare FeP/CF electrode before etching in acid is completely covered by a phosphate and/or oxide layer based on the spectrum in the P 2p region (Figure S12) in which the peak related to the metal phosphide is absent. These superficial oxygenated species are at least partly removed after the acid etching, as was previously observed after immersing the electrodes in HCl solution.[18] Then, this pretreatment enhances the direct presence of metal phosphide at the surface. By analyzing Figure 6, it is evident a higher surface concentration of phosphates in the electrode measured in the alkaline electrolyte. The formation of iron phosphate may be favored

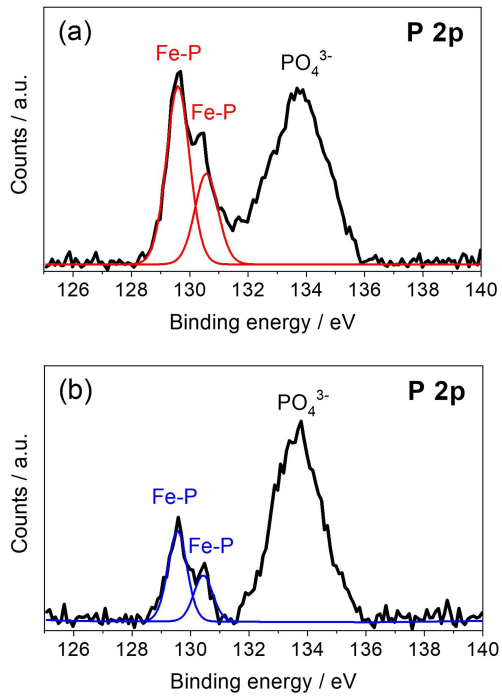

Figure 6. XPS spectra in the P 2p region for FeP/CF electrodes after HER at 100 mA·cm^{-2} in (a) 0.5 M H_2SO_4 and (b) 1 M KOH electrolyte.

under these conditions when the cathodic bias is removed. Nevertheless, the XPS analysis demonstrates that FeP remains at the electrode surface after the HER at such high current densities of 100 mA·cm^{-2} in both pH conditions. The P/Fe ratio found by XPS is 2.7 and 1.7 in the electrodes measured in acid and alkaline electrolyte, respectively, which indicates that the electrode surface is enriched with phosphorous.

Commercial PEM electrolyzers typically work at 500–1000 mA·cm^{-2}, reaching higher hydrogen production rates than alkaline-based electrolyzers. For evaluating the potential of the FeP/CF cathodes in such conditions, the stability of the FeP/CF electrodes was measured at 1 A·cm^{-2} and 50 °C in both acidic and alkaline electrolytes (Figure S13). In the acidic electrolyte, the cyclic voltammetries before and after the stability test (Figure S14a) present the same j-V curve that is indicative of good stability. Additionally, the capacitive currents in the region without faradaic processes (above 0 V vs RHE) are unaltered (Figure S14b), which may indicate that there is any significant change in the electrochemical surface area after the chronoamperometry. In both electrolytes, after 2 h at 1 A·cm^{-2}, the peaks of FeP are present in the XRD patterns (Figure S15) and the presence of iron and phosphorous was further corroborated by EDX. However, for 1 M KOH, two new peaks appear in the pattern that are in agreement with the presence of metallic iron. This indicates that despite the good stability of the current with time, the electrode undergoes chemical changes under these conditions.

Electrochemical performance of the FeP/CF cathodes in a PEM electrolyzer prototype

The previous results in three-electrode configuration are useful to investigate the electrochemical properties of the electrodes toward the desired reaction in controlled conditions. However, testing the electrochemical performance in a flow cell is the next step for the evaluation of the industrial application of the fabricated electrodes. Also, the use of polymeric membranes is advisable for more efficient separation of the produced gases, allowing the hydrogen gas to be obtained with higher purity. For this goal, FeP/CF electrodes were tested in the PEM flow cell prototype depicted in Figure 7a. A commercial membrane electrode assembly (MEA) composed of $IrRuO_x$ anode and a Nafion 115 membrane is arranged in zero-gap with the FeP/CF cathode in contact with the graphite current collector. This configuration allows for minimizing the electrolyte resistance through the cell, which is critical for achieving a low applied voltage, i.e., high cell efficiency. Figure 7b shows the resulting cyclic voltammograms in two-electrode configuration using this small prototype with a geometric area in the cathode of 1.8 cm^2 and a deposited area of $IrRuO_x$ of 10 cm^2. At room temperature, the applied potentials to achieve 100 and 800 mA·cm^{-2} are 1.85 V and 2.75 V, respectively, while after IR correction they are 1.77 V and 2.17 V, respectively. After increasing the temperature to 50 °C the potentials are reduced to 1.75 V and 1.68 V (IR-

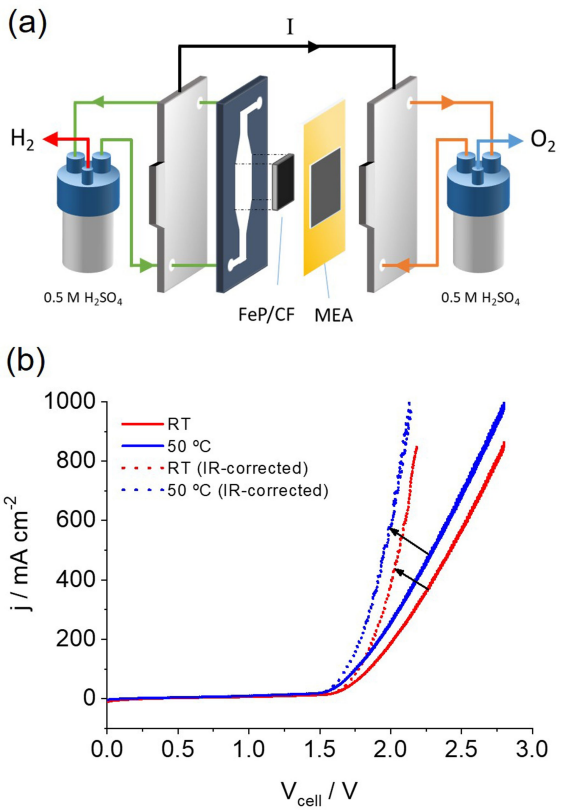

Figure 7. (a) Sketch of the PEM cell configuration, using an FeP/CF electrode of 1.8 cm^2 and anodic area of 10 cm^2 (b) Cyclic voltammograms at 50 mV·s^{-1} in the positive-going scan in the PEM cell in (a) with and without IR correction at room temperature (RT) and 50 °C.

corrected) for 100 $mA \cdot cm^{-2}$ and 2.62 V and 2.07 V (IR-corrected) for 800 $mA \cdot cm^{-2}$. This excellent performance is competitive with the values of the literature for metal phosphides,[30] corroborating the suitability of the selected FeP/CF cathodes in PEM cells. Furthermore, the stability of the cell was tested at an applied voltage of 1.69 V. The cyclic voltammograms before and after 1 h of HER present similar j-E characteristic curves (Figure S16), which indicates good stability of the components of the cell. These results are promising for a potential industrial application of the developed cathodes for the HER and will motivate further studies in the optimization of the configuration and the scaling up of the device. In addition, the combination with a MEA containing an Earth-abundant-based anode is advisable for reducing the device fabrication costs.

Conclusion

In this work, we develop a 3D cathode consisting of FeP and a carbonaceous support (carbon felt) that shows outstanding water electrolysis performance in a PEM cell. Remarkably, the fabricated electrode is only composed of Earth-abundant elements. It displays low Tafel slopes and ultralow overpotentials for the HER of only 41 and 63 mV in acidic and alkaline electrolytes, respectively, to generate 10 $mA \cdot cm^{-2}$. Such high performance is ascribed to the good electron transport through the electrode, and the homogenous deposition of FeP nanoparticles on the carbon support with a high coverage leading to a high number of exposed active sites. This was achieved by devising a careful synthesis procedure. The favorable conductive interface was obtained by using Fe_2O_3 nanoparticles directly grown on the carbon fibers as a sacrificial intermediate material for the generation of FeP without the use of any binder. The FeP/CF electrode retains impressive electrochemically active areas of more than 4000 cm^2 while the TOF was ~0.4 s^{-1} at an overpotential of 100 mV. Additionally, the FeP/CF electrode exhibits excellent stability and the FeP phase was preserved after HER at 100 $mA \cdot cm^{-2}$ in both acid and alkaline media. Reaching higher current densities of 1 $A \cdot cm^{-2}$ is facilitated by the 3D structure of the employed carbon scaffold, with adequate porous size for gas bubbles release. Due to the potential of these electrodes for practical energy conversion devices, they were combined with a membrane electrode assembly in zero-gap configuration in a small electrolyzer prototype. The device reached high hydrogen productivity of 14.9 mmol $H_2 \cdot h^{-1} \cdot cm^{-2}$ with a current density of 800 $mA \cdot cm^{-2}$ at only 2.1 V in acidic electrolyte. This work demonstrates that the developed low-cost electrode is promising for industrial PEM electrolyzers for high hydrogen productivity by a feasible scaling up toward higher electrodic areas.

Experimental Section

Electrode preparation: FeP/CF electrodes were prepared by a two-step synthesis. In the first step, an ink was prepared by dissolving 20 wt.% $Fe(NO_3)_3 \cdot 9H_2O$ and 2.5 wt.% polyvinylpyrrolidone (molecular weight of 40000) in N,N-Dimethylformamide and heating at 70 °C for 20 min under vigorous stirring.[14] Round pieces of CF (GFD 2.5 EA, SGL Carbon) of 1 cm in diameter (geometric area of 0.785 cm^2) were dip-coated in this precursor solution, and subsequently, the ink excess was removed. Afterward, they were dried at 150 °C and then heated at 400 °C for 1 h in air leading to the Fe_2O_3/CF electrodes. In the second step, they were placed in a porcelain boat with $NaH_2PO_2 \cdot H_2O$ (Alfa Aesar) in separate positions and then introduced in a tubular oven. Before heating, Ar gas was flowing for 1 h at room temperature to remove the oxygen inside the oven tube. Then, the temperature was raised to 350 °C and kept for 1 h using a low Ar flux that was estimated to be around 5 $mL \cdot min^{-1}$ leading to the FeP/CF electrodes (caution: toxic PH_3 gas is generated during the decomposition of NaH_2PO_2. PH_3 self-ignites in air, so the reaction should be performed under air-free conditions).

Physicochemical characterization: Structural characterization was performed by XRD using a D8 Advance Bruker diffractometer equipped with a Cu Kα (1.5406 Å) radiation source, LYNXEYE super speed detector and Ni filter. A Bragg–Brentano (θ–2θ) configuration was used with a step size of 0.025°. The morphology of the electrodes was analyzed by an XHRSEM Magallan 400 L equipment. Both the HRTEM and scanning TEM (STEM)-EELS were obtained in FEI F20 STEM microscope operated at 200 kV. The HRTEM was acquired with a condenser aperture of 100 μm, no objective aperture, spot size 3 and using a BM-UltraScan CCD camera. The STEM-EELS was acquired with a condenser aperture of 70 μm, no objective aperture, a nominal camera length of 30 mm, spot size 6, and using a Gatan QUANTUM GIF spectrometer. The same conditions apply for STEM-EDX, with a detector EDAX super ultra-thin window (SUTW) X-ray detector, 136 eV resolution ($Z > Z(Be)$), detector area of 30 mm^2. For these measurements, part of the FeP/CF electrode was scratched off and mixed with hexane. Before the analysis, the dispersion was sonicated in an ultrasonic bath, then deposited on a grid and dried at 50 °C. Core level XPS photoemission spectra were registered in normal emission mode at room temperature by using a NEXSA X-ray Photoelectron Spectrometer (Thermo-Scientific) using a monochromatic Al Kα line as an X-ray source.

Electrochemical characterization: The study of the electrochemical activity of the FeP/CF electrodes was carried out in a three-electrode cell. All the potentials were measured against an Ag/AgCl/KCl reference electrode. The potentials against the reversible hydrogen electrode (RHE) in acidic electrolyte were estimated in three-electrode cell using 0.5 M H_2SO_4 electrolyte saturated with high purity H_2 and a Pt wire as a working electrode, leading to $E(vs\ RHE) = E(vs\ Ag/AgCl) + 0.230$ V. In alkaline media, the potentials vs RHE were calculated as $E(vs\ RHE) = E(vs\ Ag/AgCl) + 0.205 + 0.059$ pH. The electric contact with the FeP/CF electrodes was performed with a Ta wire clip. To evaluate HER, linear sweep and cyclic voltammetries were recorded at a scan rate of 2 $mV \cdot s^{-1}$ in 0.5 M H_2SO_4 or 1 M KOH under stirring at 300 rpm. All the potentials were corrected with the IR drop, and the corresponding resistance, R, was determined by electrochemical impedance spectroscopy (EIS). Before all the electrochemical measurements, the electrodes were etched in 0.5 M H_2SO_4 for 30–60 min to remove impurities. For the analysis in 1 M KOH solution, after the etching, the electrode was washed with water and then kept for 1 h in 1 M KOH solution. Measurements for ECSA and TOF were performed after a cyclic voltammetry in the HER potential region up to cathodic current density of 150 $mA \cdot cm^{-2}$ in 0.5 M H_2SO_4. Full flow cell measurements were performed in a two-electrode configuration, with the FeP/CF electrode (1.8 cm^2) in zero-gap with a MEA composed of Nafion 115 and 4 mg cm^{-2} $IrRuO_x$ catalyst (10 cm^2, The Fuel Cell Store). 0.5 M H_2SO_4 electrolyte was recirculated in the cathode and anode in two independent bottles at about 60 $mL \cdot min^{-1}$. In this case, linear sweep voltammograms were recorded at 50 $mV \cdot s^{-1}$.

Acknowledgements

M.I. acknowledges the support from Ministerio de Ciencia e Innovación in Spain through Juan de la Cierva fellowship (FJC2018-036229-I). The authors extend their overall appreciation to the Deputyship for Research & Innovation, Ministry of Education in Saudi Arabia for funding this research work through the project number DRI 598. The project on which these results are based has received funding from the European Union's Horizon 2020 research and innovation programme under Marie Skłodowska-Curie grant agreement No. 801342 (Tecniospring INDUSTRY) and the Government of Catalonia's Agency for Business Competitiveness (ACCIÓ). ICN2 and IREC acknowledge funding from Generalitat de Catalunya 2021 SGR 00457 and 2021 SGR 01581, respectively. The authors thank support from the projects NANOGEN (PID2020-116093RB–C43) and CERES (PID2020-116093RB–C42) funded by MCIN/AEI/10.13039/501100011033/and by "ERDF A way of making Europe", by the "European Union". This study was supported by MCIN with funding from European Union NextGenerationEU (PRTR–C17.I1) and Generalitat de Catalunya. ICN2 is supported by the Severo Ochoa program from Spanish MCIN / AEI (Grant No.: CEX2021-001214-S). ICN2 and IREC are funded by the CERCA Programme/Generalitat de Catalunya. Part of the present work has been performed in the framework of Universitat Autònoma de Barcelona Materials Science PhD program. M.B. acknowledges support from SUR Generalitat de Catalunya and the EU Social Fund; project ref. 2020 FI 00103. The authors thank M. Rosado for the technical support on the electron microscopy measurements.

Conflict of Interest

The authors declare no conflict of interest.

Data Availability Statement

Research data are not shared.

Keywords: carbon felt · hydrogen evolution reaction · FeP nanoparticles · PEM electrolyzer · water splitting

[1] A. Marshall, B. Børresen, G. Hagen, M. Tsypkin, R. Tunold, *Energy* **2007**, *32*, 431.
[2] S. Siracusano, V. Baglio, N. Briguglio, G. Brunaccini, A. Di Blasi, A. Stassi, R. Ornelas, E. Trifoni, V. Antonucci, A. S. Aricò, *Int. J. Hydrogen Energy* **2012**, *37*, 1939.
[3] C. Lo Vecchio, S. Trocino, S. C. Zignani, V. Baglio, A. Carbone, M. I. Díez-García, M. Contreras, R. Gómez, A. S. Aricò, *Catalysts* **2020**, *10*, 525.
[4] Z. Zakaria, S. K. Kamarudin, *Int. J. Energy Res.* **2021**, *45*, 18337.
[5] S. Xu, H. Zhao, T. Li, J. Liang, S. Lu, G. Chen, S. Gao, A. M. Asiri, Q. Wu, X. Sun, *J. Mater. Chem. A* **2020**, *8*, 19729.
[6] S. T. Oyama, *J. Catal.* **2003**, *216*, 343.
[7] P. Xiao, W. Chen, X. Wang, *Adv. Energy Mater.* **2015**, *5*, 1500985.
[8] Y. Pei, Y. Cheng, J. Chen, W. Smith, P. Dong, P. M. Ajayan, M. Ye, J. Shen, *J. Mater. Chem.* **2018**, *6*, 23220.
[9] Y. Li, Z. Dong, L. Jiao, *Adv. Energy Mater.* **2020**, *10*, 1902104.
[10] R. Koutavarapu, C. Venkata Reddy, B. Babu, K. R. Reddy, M. Cho, J. Shim, *Int. J. Hydrogen Energy* **2020**, *45*, 7716.
[11] J. Liu, M. Meyns, T. Zhang, J. Arbiol, A. Cabot, A. Shavel, *Chem. Mater.* **2018**, *30*, 1799.
[12] X. Zhao, X. Kong, Z. Liu, Z. Li, Z. Xie, Z. Wu, F. He, X. Chang, P. Yang, J. Zheng, X. Li, *Nano Today* **2021**, *40*, 101245.
[13] Y. Liang, Q. Liu, A. M. Asiri, X. Sun, Y. Luo, *ACS Catal.* **2014**, *4*, 4065.
[14] J. Tian, Q. Liu, Y. Liang, Z. Xing, A. M. Asiri, X. Sun, *ACS Appl. Mater. Interfaces* **2014**, *6*, 20579.
[15] Y. Wang, X. Wang, L. Zhang, Y. Zhang, Z. Xu, L. Lu, J. Huang, L. Yin, W. Zhu, Z. Zhuang, *Inorg. Chem.* **2022**, *61*, 2954.
[16] Y. Gao, J. Wang, J. Mou, J. Wang, J. Ma, H. Ren, *Chem. Phys. Lett.* **2019**, *734*, 136740.
[17] W. L. Kwong, E. Gracia-Espino, C. C. Lee, R. Sandström, T. Wågberg, J. Messinger, *ChemSusChem* **2017**, *10*, 4544.
[18] X. Zhao, Z. Zhang, X. Cao, J. Hu, X. Wu, A. Y. R. Ng, G. P. Lu, Z. Chen, *Appl. Catal. B* **2020**, *260*, 118156.
[19] Z. Lu, L. Sepunaru, *Electrochim. Acta* **2020**, *363*, 137167.
[20] J. Ji, L. L. Zhang, H. Ji, Y. Li, X. Zhao, X. Bai, X. Fan, F. Zhang, R. S. Ruoff, *ACS Nano* **2013**, *7*, 6237.
[21] C. Yu, Z. Liu, X. Han, H. Huang, C. Zhao, J. Yang, J. Qiu, *Carbon* **2016**, *110*, 1.
[22] N. K. Chaudhari, P. Yu, B. Kim, K. Lee, J. Li, *Dalton Trans.* **2018**, *47*, 16011.
[23] X. Yang, A. Y. Lu, Y. Zhu, S. Min, M. N. Hedhili, Y. Han, K. W. Huang, L. J. Li, *Nanoscale* **2015**, *7*, 10974.
[24] Y. Yan, B. Y. Xia, X. Ge, Z. Liu, A. Fisher, X. Wang, *Chem. A Eur. J.* **2015**, *21*, 18062.
[25] D. Li, Q. Liao, B. Ren, Q. Jin, H. Cui, C. Wang, *J. Mater. Chem. A* **2017**, *5*, 11301.
[26] X. Yan, T. Chen, L. Wang, X. Li, H. Wang, B. Deng, Z. Wei, M. Qu, *ChemElectroChem* **2018**, *5*, 3293.
[27] K. J. Kim, Y. J. Kim, J. H. Kim, M. S. Park, *Mater. Chem. Phys.* **2011**, *131*, 547.
[28] Z. Tahmasebi, A. M. Zardkhoshoui, S. S. H. Davarani, *Catal. Sci. Technol.* **2021**, *11*, 1814.
[29] B. Owens-Baird, J. P. S. Sousa, Y. Ziouani, D. Y. Petrovykh, N. A. Zarkevich, D. D. Johnson, Y. V. Kolen'ko, K. Kovnir, *Chem. Sci.* **2020**, *11*, 5007.
[30] F. M. Sapountzi, E. D. Orlova, J. P. S. Sousa, L. M. Salonen, O. I. Lebedev, G. Zafeiropoulos, M. N. Tsampas, H. J. W. Niemantsverdriet, Y. V. Kolenko, *Energy Fuels* **2020**, *34*, 6423.
[31] S. Zhang, X. Zhang, Y. Rui, R. Wang, X. Li, *Green Energy & Environ.* **2021**, *6*, 458.
[32] J. Wang, F. Xu, H. Jin, Y. Chen, Y. Wang, *Adv. Mater.* **2017**, *29*, 1605838.
[33] Y. Yao, N. Mahmood, L. Pan, G. Shen, R. Zhang, R. Gao, F. E. Aleem, X. Yuan, X. Zhang, J. J. Zou, *Nanoscale* **2018**, *10*, 21327.
[34] S. Yao, V. Forstner, P. W. Menezes, C. Panda, S. Mebs, E. M. Zolnhofer, M. E. Miehlich, T. Szilvási, N. Ashok Kumar, M. Haumann, K. Meyer, H. Grützmacher, M. Driess, *Chem. Sci.* **2018**, *9*, 8590.
[35] F. Ma, C. Xu, F. Lyu, B. Song, S. Sun, Y. Y. Li, J. Lu, L. Zhen, *Adv. Sci.* **2019**, *6*, 1801490.
[36] M. Jafarian, O. Azizi, F. Gobal, M. G. Mahjani, *Int. J. Hydrogen Energy* **2007**, *32*, 1686.
[37] J. Kibsgaard, Z. Chen, B. N. Reinecke, T. F. Jaramillo, *Nat. Mater.* **2012**, *11*, 963.
[38] F. Zhou, Y. Zhou, G. G. Liu, C. T. Wang, J. Wang, *Rare Met.* **2021**, *40*, 3375.
[39] S. Anantharaj, S. R. Ede, K. Karthick, S. Sam Sankar, K. Sangeetha, P. E. Karthik, S. Kundu, *Energy Environ. Sci.* **2018**, *11*, 744.
[40] X. Zhang, X. Zhang, H. Xu, Z. Wu, H. Wang, Y. Liang, *Adv. Funct. Mater.* **2017**, *27*, 1606635.
[41] F. Yu, H. Zhou, Y. Huang, J. Sun, F. Qin, J. Bao, W. A. Goddard, S. Chen, Z. Ren, *Nat. Commun.* **2018**, *9*, 2551.
[42] J. Shi, F. Qiu, W. Yuan, M. Guo, C. Yuan, Z. H. Lu, *Electrochim. Acta* **2020**, *329*, 135185.

Manuscript received: December 20, 2022
Revised manuscript received: March 23, 2023
Version of record online: May 10, 2023